Thermal Analysis of Indirect Liquid Cooling for the Navy integrated Power Electronics Building Block

by

David E. Hernandez

Submitted to the Department of Mechanical Engineering in Partial Fulfillment of the Requirements for the Degree of

Bachelor of Science

at the

Massachusetts Institute of Technology

May 2023

© 2023 David E. Hernandez. All rights reserved.

The author hereby grants to MIT a nonexclusive, worldwide, irrevocable, royalty-free license to exercise any and all rights under copyright, including to reproduce, preserve, distribute and publicly display copies of the thesis, or release the thesis under an open-access license.

Authored by: David E. Hernandez
Department of Mechanical Engineering
May 12, 2023

Certified by: Julie Chalfant
Research Scientist
Thesis Supervisor

Certified by: Chryssostomos Chryssostomidis
Professor of Mechanical and Ocean Engineering
Thesis Supervisor

Accepted by: Kenneth Kamrin
Associate Professor of Mechanical Engineering
Undergraduate Officer

Thermal Analysis of Indirect Liquid Cooling for the Navy Integrated Power Electronics Building Block

by

David E. Hernandez

Submitted to the Department of Mechanical Engineering on May 12, 2023 in Partial Fulfillment of the Requirements for the Degree of Bachelor of Science

ABSTRACT

The development of the Navy integrated Power and Energy Corridor (NiPEC) involves the deployment of modular, self-contained universal converter units known as the integrated Power Electronics Building Blocks (iPEBB). An iPEBB unit sees primary heat generation through four rows of MOSFET switches and a transformer, which produce 9600W and 1100W of waste heat respectively. In response to the Navy's prohibition of direct liquid cooling, indirect liquid cooling, which sees the iPEBB unit in dry contact with a liquid-cooled cold plate, has been chosen as a potential thermal solution. A half-iPEBB thermal model was created and tested in steady state using computational fluid and thermal simulation. The chosen cold plate design using a flow rate of 8.4 gpm and inlet temperature of 25°C was found to reduce MOSFET temperatures to a maximum of 148°C, providing 2°C of margin to operational limits. Heat pipes were explored to counter the high temperatures (>100°C) seen within the ferrite transformer core, resulting in highs between 82°C and 118°C for the range of possible ferrite thermal conductivities. This preliminary analysis confirms the viability of indirect liquid cooling for the MOSFET switches of the iPEBB unit and provides insight into the design of the cooling solution for the transformer core. These findings will inform the requirements of the system-level cooling solution and offer a reference for future experimental testing of the iPEBB unit.

Thesis Supervisor: Julie Chalfant
Title: Research Scientist

Thesis Supervisor: Chryssostomos Chryssostomidis
Title: Professor of Mechanical and Ocean Engineering

Table of Contents

Abstract 2

Table of Contents 3

List of Figures 4

List of Tables 4

Acknowledgements 4

1. Introduction 5

2. Background 6

- **2.1** iPEBB 6
- **2.2** SiC MOSFET Bridges 8
- **2.3** Transformer 9
- **2.4** Common Substrate 10
- **2.5** Thermal Interface Pad 11
- **2.6** Cold Plate 12
- **2.7** Heat Pipe Theory 13

3. Thermal Model 15

- **3.1** Material Properties 15
- **3.2** Heat Load Modeling 16
- **3.3** Heat Pipe Modeling 17
- **3.4** Boundary Conditions and Simulation Settings 20

4. Results and Discussion 21

5. Conclusion and Future Work 25

References 27

Appendices 29

- **Temperature-dependent Thermal Conductivity Tables for Selected Materials** 29
- **Resistor Network for Transformer Cylinder Core (with Side Heat Pipes)** 30
- **Temperature-dependent Properties for Deionized Water** 32

List of Figures

Figure 1: iPEBB Unit and Rack-level View 6
Figure 2: iPEBB Composition Breakdown 7
Figure 3: MOSFET Switches Overview and Geometry 8
Figure 4: Transformer Geometry and Configuration 9
Figure 5: Exploded View of Common Substrate 10
Figure 6: Depiction of TIM Application 11
Figure 7: PGS Thermal Conductivity vs Applied Pressure 12
Figure 8: Fluid Flow of Cold Plate Configuration 13
Figure 9: Depiction of Heat Pipe Structure and Operation 14
Figure 10: Cross-sectional View of the MOSFET-Substrate Interface 16
Figure 11: Transformer Core Heat Generation Distribution 17
Figure 12: Depiction of Side Heat Pipes Concept 17
Figure 13: Depiction of Imbedded Heat Pipes Concept 19
Figure 14: iPEBB Thermal Model with Computational Domain 20
Figure 15: Baseline Results, MOSFETS 21
Figure 16: Baseline Results, Core 22
Figure 17: Side Heat Pipes Results 23
Figure 18: Imbedded Heat Pipes Results 24
Figure 19: 4 Heat Pipe Configuration Results 24

List of Tables

Table 1: Material Properties of iPEBB Thermal Model 15

Table 2: Simulation Results for Varying Inlet Water Temperatures 22

Table 3: Simulation Results for Varying Application Pressures 22

Table 4: Simulation Results for Heat Pipe Study 23

Acknowledgements

I would like to thank Dr. Chalfant and Prof. Chryssostomidis for their support and guidance throughout the development of this undergraduate thesis. I would also like to extend my gratitude to Mr. Ravisekhar Raju of Fast Watt LLC for his expertise and support regarding the analysis of the iPEBB transformer. Lastly, I would like to thank my parents for their continued support which has allowed me to pursue my education.

This material is based upon research supported by the U.S. Office of Naval Research (ONR) under award number ONR N00014-21-1-2124 Electric Ship Research and Development Consortium; and by the National Oceanic and Atmospheric Administration (NOAA) under Grant Number NA22OAR4170126-MIT Sea Grant College Program.

1. Introduction

The past century has seen rising naval ship capabilities push the requirements of onboard power demands, with the United States Navy estimating that the current typical ship output of 10MW will multiply to over 80MW within the next half century [1]. In order to meet the rising demands of next-generation technologies, the Navy is pursuing the development of an electric naval force. The goal is to produce a framework for an electric ship that improves power distribution and capacity while lowering the maintenance and manpower demands of current vessels. Through the Office of Naval Research (ONR), the Electric Ship Research and Development Consortium (ESRDC) has worked to achieve this goal through the development of integrated electronic power systems [2].

Current work has been focused on the Power Electronic Power Distribution Systems (PEPDS), which aims to create a robust electrical system that utilizes modern high-power components to supply both AC and DC signals to wherever they are needed throughout the ship [3]. By accommodating all potential types of electrical loads, PEPDS will allow for the consolidation of ship energy systems into one inter-connected network, enabling redundancy between zones. The PEPDS framework seeks to capitalize on this robustness to create a universal, scalable power corridor known as the Navy integrated Power and Energy Corridor (NiPEC), which will house all main electrical distribution and conversion components. Future ships will be designed from the onset to accommodate this corridor, allowing for critical bus components to be placed in locations that reduce the complexity of inter-zone connections and ensure survivability.

NiPEC is designed to consist of stacks of modular subunits called the Navy integrated Power Electronics Building Block (iPEBB). The iPEBB is designed to be a power-dense, self-contained, replaceable unit capable of providing universal power conversion needs when grouped with other iPEBB units [4]. This methodology greatly improves the resilience of the ship's electrical system, as multiple subsections of the corridor will be capable of meeting the power demands of any failed section. At a section level, relying on multiple iPEBBs ensures that the failure of any one unit does not completely eliminate power distribution to the connected components. The plug-and-play design of the iPEBB also allows for quick and easy replacement of any unit by the ship's crew, reducing the complexity of system repairs.

In order to meet the robust distribution and conversion requirements, the iPEBB makes use of high-power semiconductors that produce 9.6kW of heat loads that must be regulated in order to maintain critical electronics below 150°C [4]. In addition, a high-frequency transformer with heat losses of 1.1kW must also be managed. Cooling the iPEBB presents a significant thermal challenge, as the easily removable nature of the unit has resulted in Navy prohibitions on traditional direct liquid cooling methods. Recent work has identified indirect liquid cooling through a detached cold plate as a potential thermal solution [5]. This design would allow for a leak-proof, liquid-driven heatsink that does not contribute to the weight of the iPEBB unit.

This study will seek to investigate the feasibility of an indirect-liquid cooling solution for the iPEBB unit. A cold plate design derived from a previous thesis will be used. A thermal model of the iPEBB with its cold plate will be created for the usage of computational fluid and thermal analysis in Solidworks Flow Simulation. The goal is to determine the cooling performance under worst-case loads and varying levels of physical contact between the cold plate and iPEBB surface.

The results from this analysis will be used to inform the thermal requirements of future design iterations as well as offer a baseline for experimental validation of the cooling solution.

The remainder of the thesis will be organized as follows. First, section 2 will give an overview of the functionality and purpose of the iPEBB, as well as provide context for its various subcomponents. Next, section 3 will explore the construction of the iPEBB thermal model and review the steps taken to ensure the accurate portrayal of the unit. Section 4 will contain images and tables of the simulation results as well as a discussion of the implications of the data. Lastly, Section 5 will summarize the findings of this research and provide insight into next steps for the thermal analysis of the iPEBB.

2. Background

In order to ensure high quality results, it is critical to accurately capture the thermal properties and behaviors of the iPEBB and its components. This section will provide an overview of the assumptions and thermal requirements of the relevant heat-generating electronics, as well as those of bodies that influence the flow of heat in the system.

2.1 iPEBB

The current design of the NiPEC architecture calls for the usage of “rack” configurations, where iPEBB units are stacked vertically in order to achieve the number required for a given subsection’s power demands. Similar to a computational server storage rack, iPEBB units are designed to be removable and replaceable in the case of failure or required maintenance. In order to achieve ease of handling, the weight of the iPEBB is restricted to a maximum of 35 lbs. Similarly, the external footprint of the unit is designed to allow for quick maneuvering through naval ship corridors, with the current iteration having outer dimensions of 550mm x 300mm x 100mm, as shown in Figure 1.

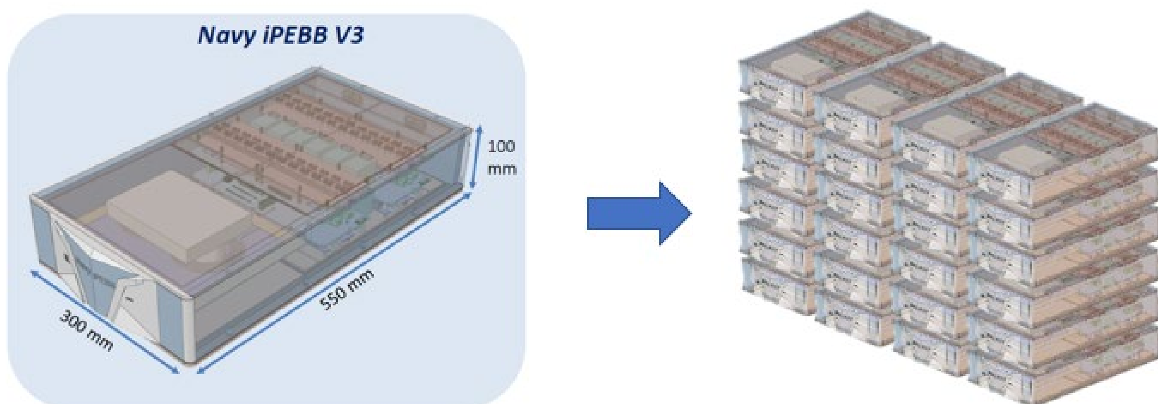

Figure 1: (Left) Isometric view of the Navy iPEBB. Exterior casing dimensions shown in mm. (Right) Depiction of iPEBBs in a stacked “rack” configuration. Number of iPEBBs and stacks can be scaled to meet the power demands of the specific subsection of the ship. Planned mounting and cooling hardware are not depicted in the image [4].

The dominant sources of heat generation within the iPEBB consist of 96 MOSFET switches and 1 high-frequency transformer, resulting in a total waste heat generation of approximately 10.7kW. A cross section view of the iPEBB internals can be seen in Figure 2. Due to restrictions on direct liquid cooling, the current design relies on the solid conduction of heat through the iPEBB baseplate, also known as the common substrate, to the outer top and bottom surfaces of the unit, which act as the de facto heatsinks for the assembly. The iPEBB must be able to maintain components under their maximum temperature limits in order to prevent performance throttling and potential electronic damage. With the high-stakes wartime scenarios that connected loads will experience, reduced performance is not an option. In order to adequately meet thermal requirements, this study will use the previously proposed concept of indirect liquid cooling, which consists of a fluid-chilled cold plate in direct contact with the outer iPEBB surfaces. The presence of a regulated low-temperature heatsink aims to improve the flow of heat through solid conduction and ensure sufficient temperature margin for the critical heat-producing components.

The main limitations faced in iPEBB cooling are currently unit weight and size requirements. The current iPEBB iteration weighs 31 lbs without the inclusion of thermal management hardware, leaving less than 4 lbs of on-unit weight for a cooling solution [4]. In addition, the chosen heatsink solution must be of reasonable size to maintain the ease of handling by human operators, as well as not interfere with current plans for the aforementioned rack configuration. It is preferred that the development of a cooling solution does not require any weight reduction or major design overhaul to the current iPEBB unit. The following subsections will go into further detail regarding the thermal characteristics and limitations of the components within the iPEBB.

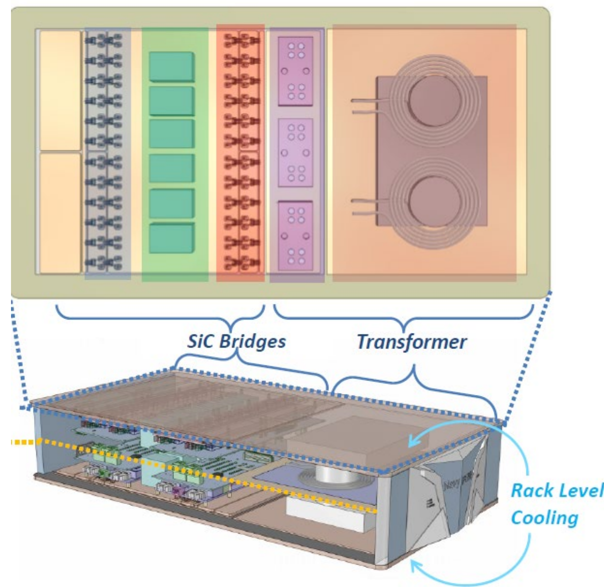

Figure 2: Top cross-section view of an iPEBB half-shell with the regions containing the main heat generating components highlighted (SiC MOSFET switches/bridges in red and blue, transformer in orange). The iPEBB consists of two symmetrical shells mirrored vertically about the yellow dotted line. The geometry and heat loads of the top and bottom subassemblies are identical. The two outer surfaces of the substrate shells, labeled in cyan, are designed for conduction to the rack-level cooling solution, which for this study consists of an aluminum cold plate through a thermal interface pad [4].

2.2 SiC MOSFET Bridges

The electrical layout of the iPEBB utilizes silicon carbide (SiC) MOSFET switches situated on the inside surface of the common substrate. Each MOSFET has a surface footprint of 1cm x 1cm, with the base of the component being mounted to the substrate through a sintered-silver connection of less than 30% porosity. Each half of the iPEBB unit contains 48 MOSFET switches in a two-row layout, with a spacing of 2cm between each unit. The MOSFET configuration can be seen in Figure 3. As both halves of the iPEBB are identical, there are a total of 96 MOSFET switches in the unit.

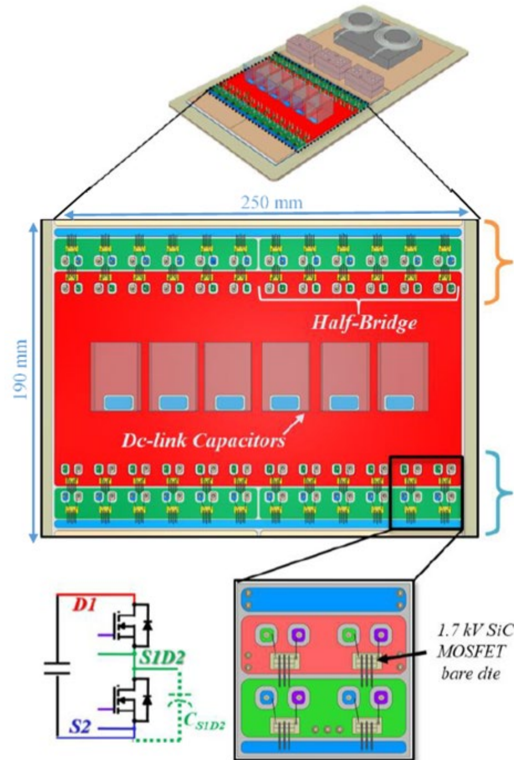

Figure 3: Top view of the iPEBB half-substrate with the SiC MOSFET switches shown in a two-row configuration. There are 48 switches mounted onto the substrate, with the other mirrored half of the iPEBB containing an additional identical set [6].

The MOSFET switches dissipate waste heat when in operation, and for the iPEBB unit are estimated to produce a worst-case load of 100W each under full load. This includes the maximum estimates for both conduction and switching losses, both of which will be considered simultaneously for this study as the goal is to safely ensure adequate thermal margin under the edge cases. This translates to 4800W of MOSFET losses per iPEBB half, or 9600W for the entire unit. The maximum component temperature limit to prevent damage to the SiC MOSFET switches is 180°C; however, for this study a safety margin of 30°C will be applied, resulting in a model upper limit of 150°C. Due to the quantity of MOSFET switches and their close proximity to one another, it is likely that the heat generated by each MOSFET will overlap with those around it, resulting in the units experiencing concentrations of high heat flux. As the MOSFETs are restricted to using conduction as the direct form of heat transfer, this will require strong cooling from the proposed cold plate to ensure that component temperatures can be managed.

2.3 Transformer

The second source of notable heat generation within the iPEBB is the high-frequency transformer. The current electrical layout contains one transformer per iPEBB unit, which consists of a Ferrite N49 core, copper coils, and an insulating mica sheet. The transformer is also split into two identical halves, with each being mounted directly to an iPEBB half-substrate and separated by the insulating sheet. For each transformer half, the ferrite core is built from a rectangular base of dimensions 150mm x 110mm x 23mm and two cylindrical cores of diameter 50mm and height 23mm. The coils consist of 6600/46 AWG litz wire with a silk sleeving and are mounted to the insulating sheet. An overview of the transformer geometry is shown in Figure 4.

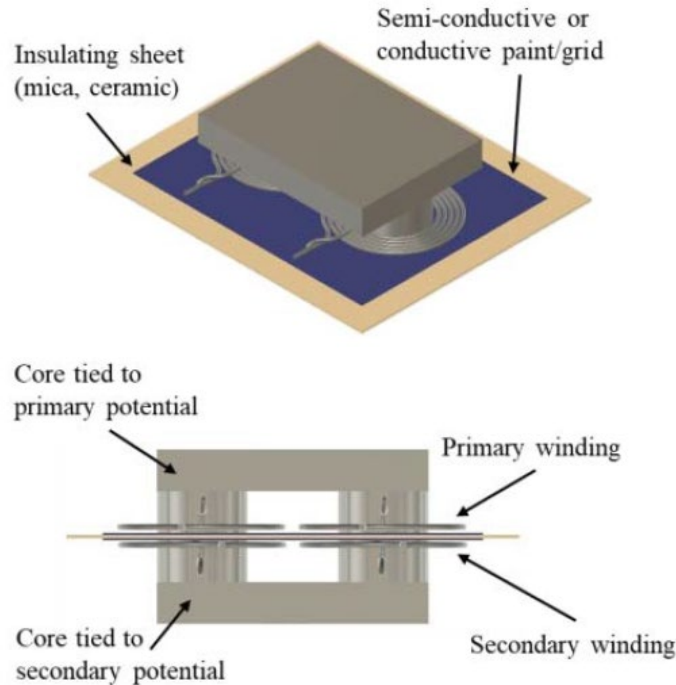

Figure 4: Overview of the current iteration of the iPEBB transformer. The top and bottom faces of the rectangular core are mounted directly to both inside iPEBB substrate surfaces. Note that the copper windings are mounted to the insulating mica sheet, and do not come into direct contact with the core material on either half [7].

The heat losses from the transformer can be split between those of the cores and coils, with both being considered secondary to the cumulative losses of the MOSFET switches. The transformer core dissipates 80W in each rectangular base and 30W in each cylindrical body, resulting in a total transformer core generation of 280W. Cooling for this load will be split evenly between the two substrate heatsinks. The temperature limits to be used for the N49 ferrite core are performance driven, as an optimal range in transformer efficiency exists at core temperatures between 60°C and 80°C, and losses rise exponentially at core temperatures over 100°C [8]. Each of the four transformer coil windings dissipates 200 W, resulting in 800 W of heat for the iPEBB. For the coils, the copper itself is only limited by its melting point of 1085°C, however the insulating materials of the litz wire have an upper temperature limit between 125°C and 175°C, with 125°C representing the conservative limit.

The current mounting design for the transformer coils to the rest of the iPEBB system remains to be determined; however, it is known that the coils will be directly mounted onto the mica sheet, which will also be in direct contact to the two transformer cores. The extremely low thermal conductivity of the mica sheet (k_{mica} = 0.75 W/m-K) results in negligible heat flow between the transformer core and coils. The primary method of cooling the transformer coils will be dependent on further design of its integration with the rest of the iPEBB system and common substrate. Due to insufficient information regarding the cooling path for the coils, this project will omit the losses generated within the coils and limit its scope to the cooling of the MOSFET switches and transformer core. Future work will investigate cooling solutions for the transformer coils.

2.4 Common Substrate

The two halves of the iPEBB unit are built upon a base panel known as the common substrate. This base is formed by alternating sheets of copper and Risho, a dielectric epoxy resin composite that will be referred to by its manufacturer's name. The copper layers serve to disperse heat generated from the electronics, whereas the Risho layers are required to ensure voltage isolation. A breakdown of the layer composition with layer thicknesses can be found in Figure 5. The outer surface of the "bottom copper" layer will be in direct contact with the indirect liquid-cooling cold plate.

As a whole, the substrate provides mechanical integrity to the iPEBB and plays a crucial role in the cooling of the components. Due to the lack of cooling medium inside the iPEBB, all of the waste heat generated will flow through the common substrate and to the cold plate mounted on the outer side. The heat flow through the Risho layers poses the largest challenge with the common substrate, as its low thermal conductivity (10 W/m-K) compared to the copper layers (398 W/m-K) will serve as the main source of thermal resistance through this body.

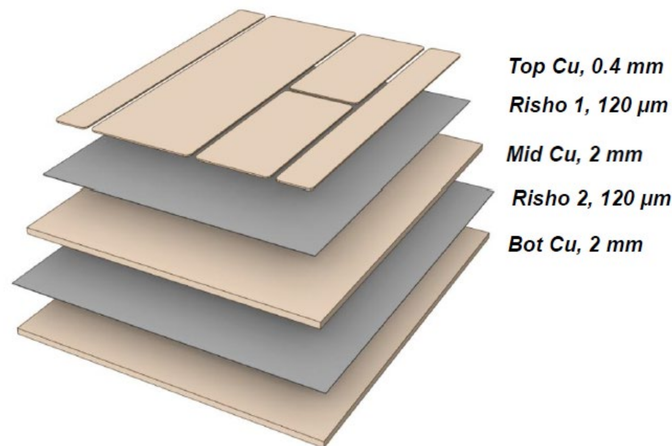

Figure 5: Exploded view of the iPEBB common substrate with layer thicknesses noted. The "bottom copper" and "Risho 2" layers extend to cover the length of the iPEBB. MOSFET switches are mounted to the upper face of the "top copper" layer. The transformer core is mounted to a second, detached, "middle copper" layer that is located to the side of the one shown [4].

2.5 Thermal Interface Pad

In order to improve heat flow between the common substrate and cold plate cooling solution, a thermal interface pad of PGS graphite will be attached directly to the shared surface. When any two solid materials are in contact, surface imperfections at the microscopic level result in the formation of voids that reduce the true contact area for heat to flow, creating a non-negligible thermal resistance. PGS graphite sheets act as a filler, being able to deform to occupy these voids and subsequently reduce the thermal resistance of the interface. This is important for the successful cooling of the iPEBB as reducing the thermal resistance from the heat-generating units to the cold plate will improve heat flow and result in lower maximum electronic temperatures. A demonstrative depiction of PGS graphite in this use-case is shown in figure 6.

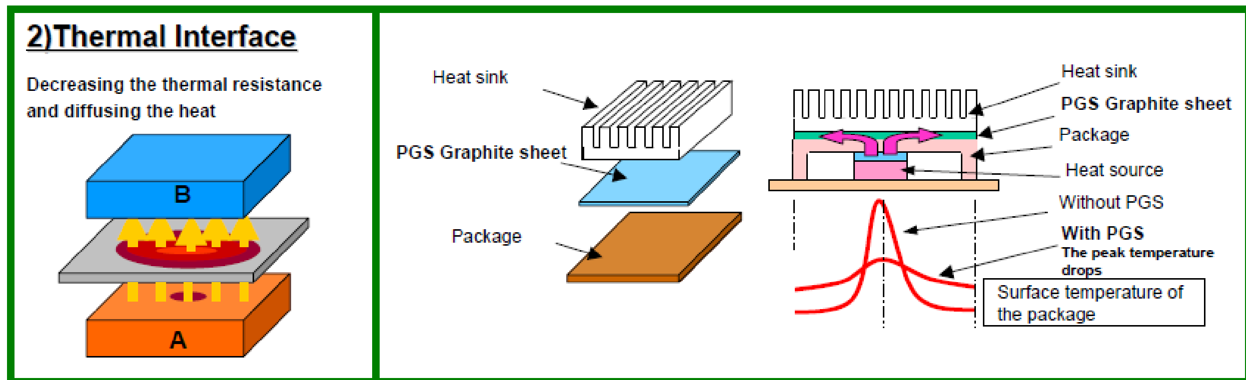

Figure 6: Vendor illustration depicting the benefits of employing a PGS graphite sheet to decrease thermal contact resistance [9].

The effective thermal conductivity of the PGS sheets, in the direction normal to the contact surfaces, varies with the pressure that is applied on them. Recent work investigating the thermal properties of this material depicts the relationship between pressure and thermal conductivity in Figure 7. The current design for the iPEBB rack mounting mechanism will apply a compressive force to the bottom and top of the iPEBB-cold plate assembly, sandwiching the PGS interface pads in the process. This thesis will consider the thermal performance of the cooling system under a range of application pressures; however, the baseline scenario will assume a uniform pressure of 10psi.

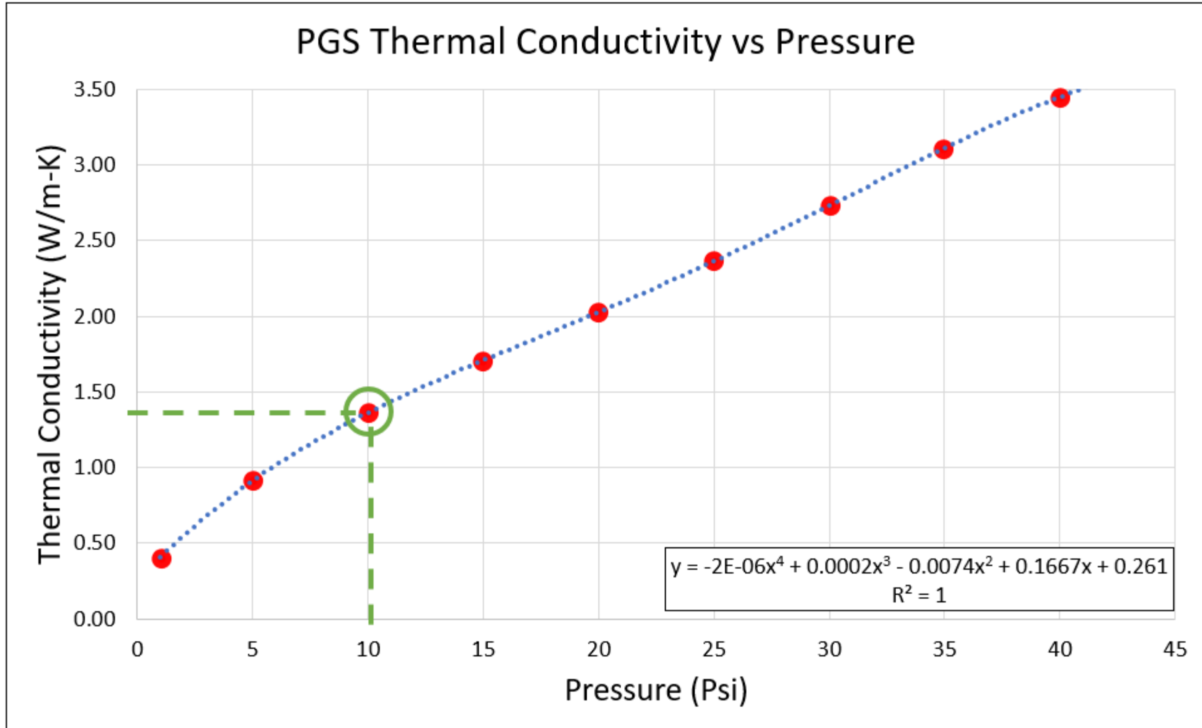

Figure 7: Thermal conductivity of PGS pads at different applied pressures, based off an experimentally determined fourth-order curve of best fit. The iPEBB unit is assumed to experience 10psi of applied pressure from the mounting mechanism, resulting in a thermal conductivity of the PGS pad of 1.36 W/m-K [10].

2.6 Cold Plate

The indirect liquid cooling concept is built around an aluminum cold plate, which sees a flow of cooled deionized water run through internal pipes to lower temperatures throughout the plate. This cold plate design is separate from the iPEBB unit itself and ensures that no fluid will be flowing to or near the critical electronic components. The performance offered by a liquid-cooled heatsink will be needed to manage the high heat fluxes seen in the iPEBB. The design used in this study was created in a previous project and utilizes a crossflow configuration within the cold plate [5]. As the cold plate is designed to be rack-mounted and detached from the iPEBB, it does not contribute to the weight or volume of the iPEBB unit itself. This feature addresses the mobility and handling limitations previously mentioned. Under this design, support structures on the rack will be needed to provide a securing mechanism for the plate, providing the 10psi clamping force onto the assembly that determines the thermal characteristics of the PGS thermal interface pad. An image of the cold plate with its internal flow is shown in Figure 8.

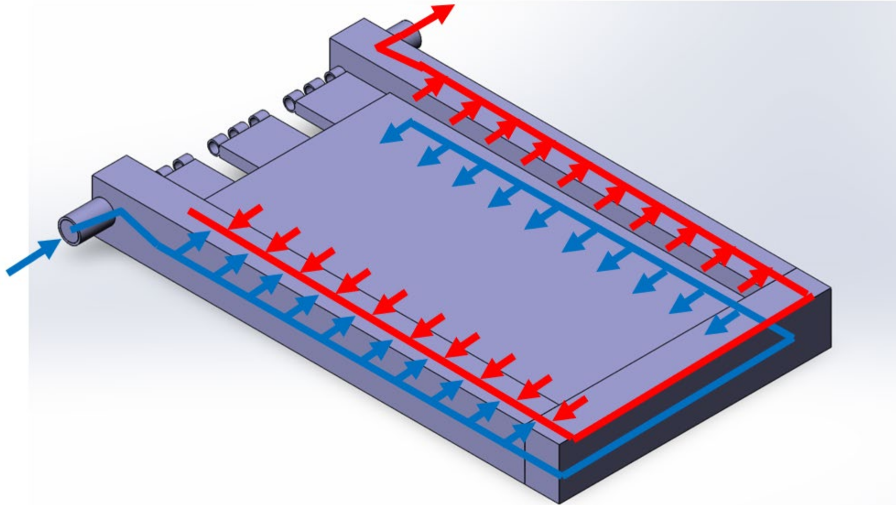

Figure 8: Current iteration of the iPEBB cold plate for an indirect liquid cooling solution. Inlet water (blue) enters the cold plate and wraps around the body to provide crossflow cooling over the center area. Warm water (red) on both sides is then routed to the outlet port. Two cold plates would be used per iPEBB unit, with one in contact with each common substrate. Note that the common substrate and thermal interface pad would be in direct contact with the recessed central rectangular area of the cold plate [5].

Current plans involve using a deionized-water closed loop dedicated to the cooling of the iPEBB cold plates in a given section. The fluid in these loops will be cooled in a local heat exchanger by the ship-wide chilled water system. Results from previous simulations estimate that a mass flow rate of 0.5245 kg/s through a cold plate inlet port is required to maintain iPEBB heat loads under their specified temperature limits [5]. In addition, analysis of the ship-wide cooling loop determined that cold plate inlet water temperatures of a range of 15°C to 35°C would be attainable [11]. Along with testing the cooling performance under various application pressures, this study will also investigate the inlet temperatures required to achieve adequate cooling performance.

2.7 Heat Pipe Theory

Heat pipes are sealed, hollowed-out tubes that utilize the phase-change of a working fluid to efficiently transfer heat from a heat source to a heatsink [12]. The structure of a heat pipe consists of an outer casing, commonly made of copper, and an internal vacuumed region with surface geometry optimized for the two-phase operation of the working fluid. The fluid, which is typically distilled water, absorbs heat in the warm end of the heat pipe until evaporation, after which the newly formed vapor travels towards the cool end of the structure and experiences condensation. The resulting heat is absorbed by the local heat pipe structure and transferred externally to the connected environment or heatsink. Meanwhile, capillary action forces the condensed fluid towards the evaporator end, creating a passive continuous cycle. A representative image of a heat pipe is shown in Figure 9.

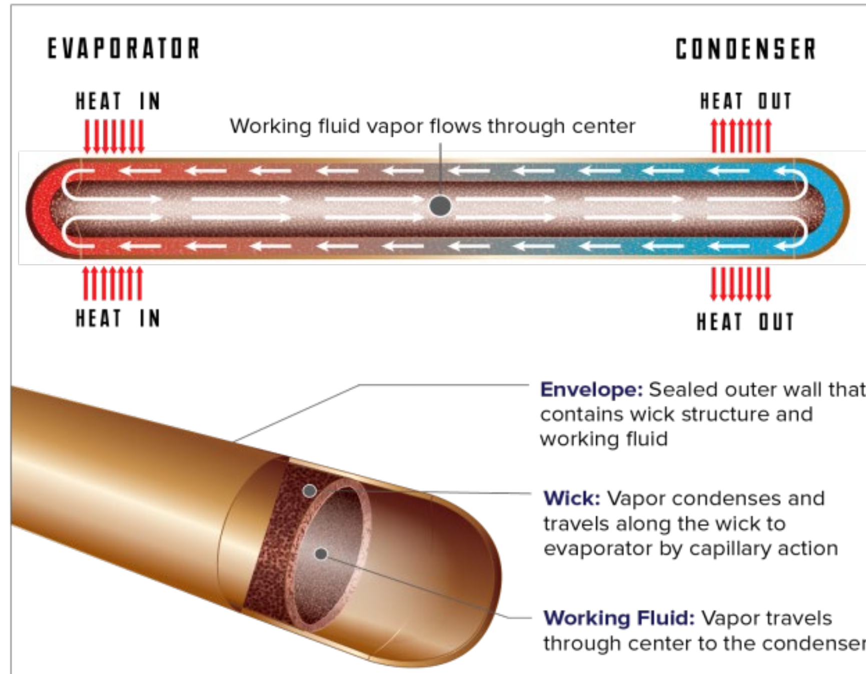

Figure 9: Depiction of a heat pipe in typical operation. The top shows the internal motion of heat and fluid. Below this is a representation of the cross-sectional geometry of the structure [12].

Heat pipes offer a low-profile, low-weight thermal management solution that can conform to various geometries and heat load situations. The usage of capillary action means that the heat pipes require no moving parts, giving long lifespans and minimal maintenance requirements. The benefits of heat pipes are reflected in their wide applications in electronic thermal management, from usage in cellular devices to spacecraft operations [13].

The usage of heat pipes in multiple configurations will be studied as a means of supplementing the cooling to the transformer core. The presence of the mica sheet, which has an extremely low thermal conductivity (k_{mica} = 0.75 W/m-K), between the two halves of the transformer core means that the common substrate serves as the only path for heat flow for the core losses. The relatively tall height of the core and low thermal conductivity of ferrite N49 ($k_{ferrite}$ = 4-7 W/m-K) creates notable thermal resistance for heat generated in these areas. There is particular concern for the cylindrical bodies of the core, as their positioning as the furthest solids from the iPEBB heatsink and heat generation of 30W each may cause high concentrations of temperature that are unable to be regulated by the cold plate alone. Heat pipes in contact with these warm regions will be tested for cooling performance within the core body.

3. Thermal Model Design

One of the benefits of computational thermal analysis is the ability to simulate the performance of a cooling solution quickly and accurately; however, the usefulness of the results is dependent on the design of an accurate model. This section will walk through the assumptions and approximations that were made in the construction of the iPEBB thermal model. The model will consist of only one-half of the iPEBB, with the performance assumed to be identical between the two symmetric halves. Following this, the results of the various tested scenarios will be shown, all of which were performed as steady-state cases within Solidworks Flow Simulation.

3.1 Material Properties

As a steady-state model is being used, thermal conductivity is the only property relevant to the solving of the simulation. All materials used, except the PGS interface pad, are modeled as isotropic. Temperature-dependent datasets within the Solidworks library exist for several of the common materials and will be used where available. These tables can be found in the appendix. For all other materials, recorded values at room temperature will be used. Material properties for all relevant bodies within the iPEBB model are shown in Table 1. Note that the transformer coils and mica sheet are omitted from this study.

Table 1: Material Properties of iPEBB Thermal Model

<table>
<tr><th>Component</th><th>Material</th><th colspan="2">Thermal Conductivity [W/m-K]</th></tr>
<tr><td>MOSFETs</td><td>Silicon Carbide (SiC)</td><td colspan="2">Temperature Dependent (Solidworks)</td></tr>
<tr><td>Transformer Core</td><td>Ferrite N49</td><td colspan="2">4 – 7 [14]</td></tr>
<tr><td>Copper Common Substrate Layers</td><td>Copper</td><td colspan="2">Temperature Dependent (Solidworks)</td></tr>
<tr><td>Risho Common Substrate Layers</td><td>Risho</td><td colspan="2">10 [4]</td></tr>
<tr><td>Thermal Interface Pad</td><td>PGS</td><td>0.91 @ 5psi
1.36 @ 10psi
1.71 @ 15psi
(through-plane) [10]</td><td>400
(in-plane) [15]</td></tr>
<tr><td>Cold Plate</td><td>Aluminum (unfinished)</td><td colspan="2">Temperature Dependent (Solidworks)</td></tr>
</table>

The material finish of the cold plate is yet to be determined; therefore, the properties of unfinished aluminum, a common option in commercial cold plates, will be used [16]. As mentioned in the background, the thermal conductivity of the PGS interface pad varies with applied pressure and will use a baseline value of 1.36 W/m-K at 10psi. Lastly, the range provided for the ferrite N49 core reflects typical values found in all ferrite materials produced by the manufacturer. Due to the large (~75%) variance in this range, all cases will be run for both the lower and higher extremes of 4 and 7 W/m-K respectively.

3.2 Heat Load Modeling

The MOSFET switches represent the largest heat-generating components within the iPEBB. Each of the 48 switches per iPEBB half will be modeled by the volume of the component baseplate, which consists of a thin rectangular prism of thickness 0.18mm and base dimensions 4.36mm x 7.26mm. This volume is given the material properties of Silicon Carbide (SiC). The geometry and pattern of the MOSFETs reflects that which was outlined in the background. Applied on each of these MOSFET bodies is a constant volumetric heat load of 100W, resulting in a uniform heat generation flux. For the results, the maximum temperature reached within any of the MOSFET volumes will be recorded.

The attachment method between the MOSFETs and the upper layer of the common substrate is a silver-based sintered interface. A cross-sectional view of the MOSFET interface is shown in Figure 10.

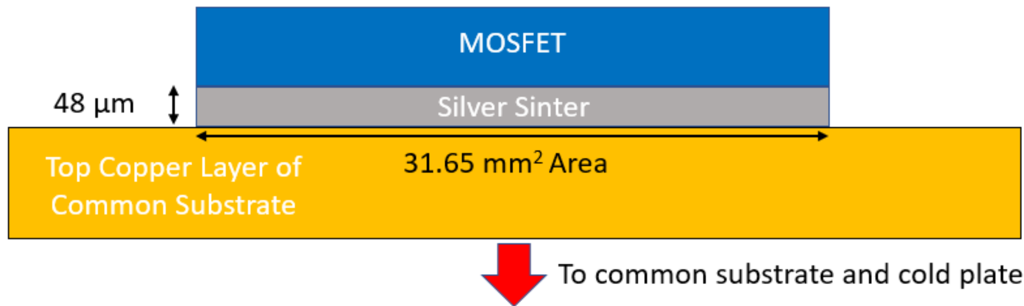

Figure 10: Cross-sectional view of the MOSFET-substrate interface with the sintered adhesion layer included. This layer is not modeled geometrically within Solidworks; however, its thermal resistance is included through the application of an effective thermal resistance at the area of contact between the MOSFET baseplate and copper layer. Dimensions are not to scale.

Whereas the thermal resistance within solids is calculated by the computational solver, the impact of this sintered layer can be captured through its effective thermal resistance. By assuming the layer is of uniform thickness, the body can be treated as a two-dimensional slab. The typical thermal conductivity of silver-based sinter with <30% porosity is estimated to be 151.6 W/m-K, and bond line thicknesses of 13-48 µm are common [17]. Using a conservative thickness value of 48 µm gives the following area-independent thermal resistance, which is applied to the area of interest.

$$R_{sinter}A = \frac{L}{k} = \frac{48\times10^{-6}m}{(151.6\frac{W}{mK})} = 3.17 \times 10^{-7}\ K \cdot m^2/W \quad (1)$$

The other heat generating component, the transformer core, has a distribution split between its individual cores and cylinders, which is visualized in Figure 11. Similar to the MOSFETs, losses are being modeled as volumetric heat loads originating from their respective bodies. Each member of the transformer core is given the material properties of Ferrite N49. Results for the transformer core will record the maximum temperature among the three bodies.

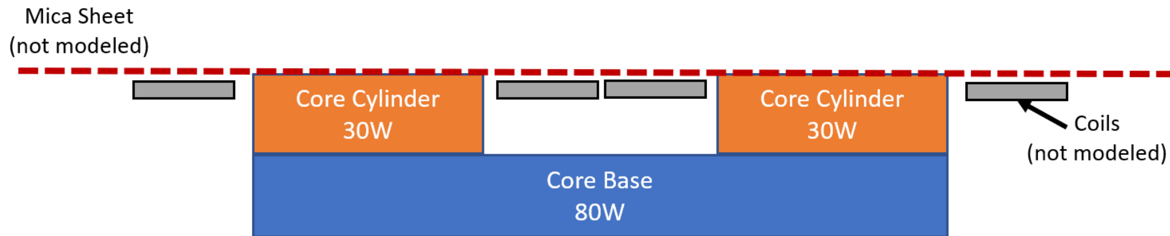

Figure 11: Breakdown of transformer core heat generation distribution for an iPEBB half-transformer. The generation of heat within each body is uniform. Mica sheet and coils are shown but are not modeled.

3.3 Heat Pipe Modeling

The first step in creating a heat pipe model was to determine the geometry and path of the design. A preliminary concept was created consisting of two 75mm-long flat-faced heat pipes, each with a cross sectional area of 11.4mm x 2.5mm. This first concept, which will be referred to as the "Side Heat Pipes" variant, places a heat pipe in contact with the side face of both transformer core cylinders and the top surface of the common substrate. This design utilizes an evaporator length (length in contact with heat source) of 14.3mm and condenser length (length in contact with heatsink) of 32.2mm. The performance potential of this geometry was validated for the operating temperatures and heat loads expected using an industry-created heat pipe modeling tool [18]. An image of the concept can be seen in Figure 12. Included in this concept is an intermediary saddle piece connecting the heat pipe to the transformer core. This copper attachment is intended to improve contact between the flat heat pipe and curved core surface, improving the flow of heat at this interface.

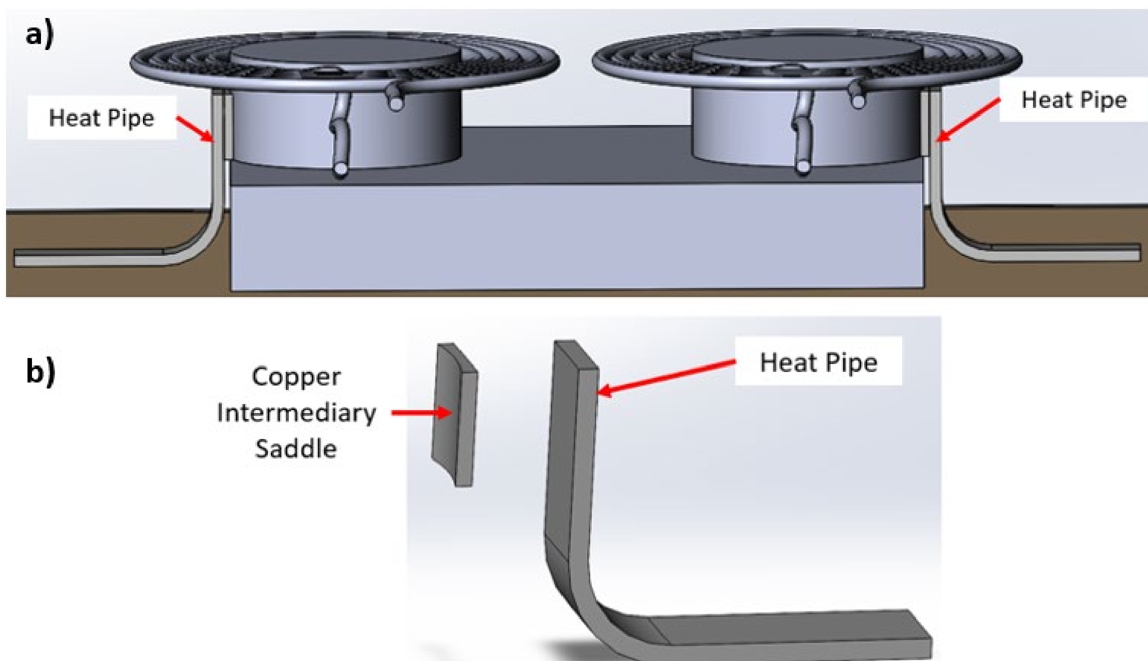

Figure 12: a) Image of the "Side Heat Pipes" concept. The transformer coils are included in this image to confirm vertical clearance to the heat pipes. b) Exploded view of the heat pipes with the copper intermediary saddle.

An analytical model was created following the process provided by Advanced Cooling Technologies (ACT) [19]. This involves splitting the heat pipe into two separate bodies within the thermal model, the inner vapor space and an outer envelope including the interior wick geometry, copper wall, solder interface, and effects of evaporation and condensation. For the heat pipe envelope, the model captures the radial resistance of the components. Using values provided from ACT for typical heat pipe properties results in the following area-independent thermal resistances:

$$R_{solder}A = \frac{L}{k} = \frac{1.02\times10^{-4}m}{(19\frac{W}{mK})} = 5.35 \times 10^{-6}\ K \cdot m^2/W \quad (2)$$

$$R_{copper}A = \frac{L}{k} = \frac{3.05\times10^{-4}m}{(380\frac{W}{mK})} = 8.02 \times 10^{-7}\ K \cdot m^2/W \quad (3)$$

$$R_{wick,evap\&cond}A = 3.20 \times 10^{-5}\ K \cdot m^2/W \quad (4)$$

Summing up the resistances and choosing the model heat pipe envelope to have a thickness of 0.04" (1.02mm) allows us to find the effective thermal conductivity of our bulk heat pipe structure.

$$k_{eff,env} = \frac{L}{(R_{solder}+R_{copper}+R_{wick,evap\&cond})A} = \frac{1.02\times10^{-3}m}{3.81\times10^{-5}K\cdot m^2/W} = 26.7\frac{W}{mK} \quad (5)$$

The effective thermal conductivity of the vapor space can be approximated when assuming a dominant direction of heat flow in the axial direction using Fourier's law. For the temperature difference, heat pipes typically see drops of about 2-5°C along their length, with 5°C representing a conservative estimate [19]. The effective length of the heat pipe is defined using the lengths of the evaporative section l_{evap}, condensing section l_{cond}, and adiabatic section l_{ad}.

$$l_{eff} = \frac{l_{evap}+l_{cond}}{2} + l_{ad} = 51.8mm \quad (6)$$

The amount of heat flow through the vapor space was estimated by accounting for the conduction path through the rectangular ferrite base and to the common substrate. The thermal resistor network for the extended model can be found in the appendix. Through iteration, an estimated 23.6W and 19.9W of heat pass through each vapor space when the ferrite core has thermal conductivities of 4 and 7 W/m-K respectively. The reason for the variance is due to the reduced thermal resistance of the core material in the 7 W/m-K case, resulting in a higher percentage of the total 30W of heat generated flowing through that path compared to the 4 W/m-K case.

Using these values, along with the known cross-sectional area of the heat pipe, allows us to arrive at the following effective thermal conductivity values for the vapor space.

$$k_{eff,vapor,4} = \frac{Q_4 l_{eff}}{A\Delta T} = 80309\frac{W}{mK} \qquad \text{(with } k_{ferrite}\text{= 4 W/m-K)} \quad (7)$$

$$k_{eff,vapor,7} = \frac{Q_7 l_{eff}}{A\Delta T} = 67844\frac{W}{mK} \qquad \text{(with } k_{ferrite}\text{ = 7 W/m-K)} \quad (8)$$

A second heat pipe concept was created with the intention of improving temperature performance of the inner regions of the transformer core cylinders. The “Imbedded Heat Pipes” concept sees two circular cross-section heat pipes placed within bored-out versions of the transformer core. These pipes have a diameter of 8mm and length of 41mm and are shown in Figure 13.

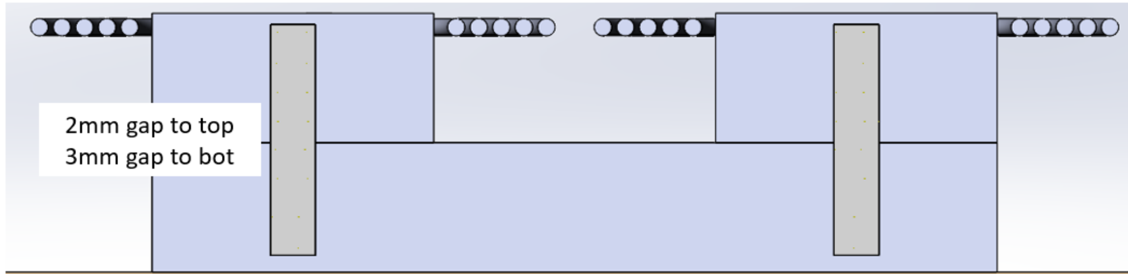

Figure 13: Image of the “Imbedded Heat Pipes” concept. The vertical clearances to the top and bottom of the core surfaces are shown.

Due to the continuous sources of heat input along the length of the heat pipes and lack of any clear “evaporator” and “condenser” lengths, a first order model was instead used to approximate this heat pipe concept. Also provided by ACT, this approach consists of modeling the heat pipe as a solid body with a high thermal conductivity that results in a 5°C temperature difference along its length [20]. For the imbedded heat pipes, an effective thermal conductivity of 1500 W/m-K was found to meet these requirements and will be used going forward. As this concept removes cross-sectional area from the bodies, additional losses in the core are expected. Following a first order estimate of the Steinmetz equation, core losses for each individual body can be estimated by the following [20]:

$$P_{core} \propto \frac{1}{A^{2.5}} \tag{9}$$

Taking the reduced areas into consideration results in losses of 32.01W in the cylinders and 81.23W in the rectangular bodies for configurations using the imbedded heat pipes.

We must also develop an effective thermal resistance for the adhesion methods not included in the current heat pipe models. For the side heat pipes, the adhesion from the copper saddle to the ferrite core was not included in the analytical heat pipe envelope modeling. Similarly, the 1st order approach for the imbedded heat pipes did not include any adhesion resistance. Thermal epoxy will be used for both interfaces, which has a typical thermal conductivity of 2.1 W/m-K and bond thickness of 15 µm [21]. This gives the following area-independent thermal resistance.

$$R_{epoxy}A = \frac{L}{k} = \frac{15\times10^{-6}m}{(2.1\frac{W}{mK})} = 7.14 \times 10^{-6}\ K \cdot m^2/W \tag{10}$$

One of the downsides of the usage of heat pipes that must be included is the induced losses generated within the copper envelope during transformer operation. The passing of electrical current through the transformer coils induces electrical flow within surrounding conductors and is responsible for the modeled losses within the ferrite transformer core [7]. This same application of Faraday’s law applies to any copper heat pipe that is placed near the areas of flux leakage, which

occur around the transformer coils. Although the heat pipe variants being tested do not fall within this area of concern, a value of 5W of heat generation within each heat pipe will be applied as a conservative estimate. Like other sources of heat generation, this value will be applied as a volumetric heat load.

3.4 Boundary Conditions and Simulation Settings

The boundary condition of most interest in the iPEBB thermal model pertains to the cooling system and flow of fluid through the cold plate. All cases use deionized water as the cooling fluid. The temperature-dependent properties of deionized can be found in the appendix.

Also shown in Figure 14 are the positions of the inlet and outlet boundaries, which were defined as the exposed faces of the two fluid connection ports. For the inlet port, a static pressure of 100psi (689 kPa) was applied along with a fluid inlet temperature of 25°C. The outlet port defines the mass flow rate through the system and is set to a value of 8.4 gpm (0.525 kg/s). Note however that these parameters define the baseline scenario, with the inlet fluid temperature being varied in one of the studies. Water temperatures of 15°C, 25°C, and 35°C will be tested for the non-heat pipe iPEBB configuration. A turbulence intensity of 2% is applied to the inlet flow to account for possible fluctuations from the mean velocity, an effect commonly seen in pipe flow.

The simulations are running as steady-state analyses, and therefore are not considering any implications of time-dependent phenomenon. A computational domain encompassing the entire solid model is used and can be seen in Figure 14. The boundaries of this domain are set to be adiabatic, preventing any additional cooling from surrounding ambient air. The flow of water is contained within the internal channels of the iPEBB cold plate. Outside of this domain there is no air or any other fluid being modeled, omitting the effects of buoyancy-driven natural convection. Radiation is also being neglected within this model, giving conservative results that rely on conduction as the sole method of heat transfer from the heat generating components.

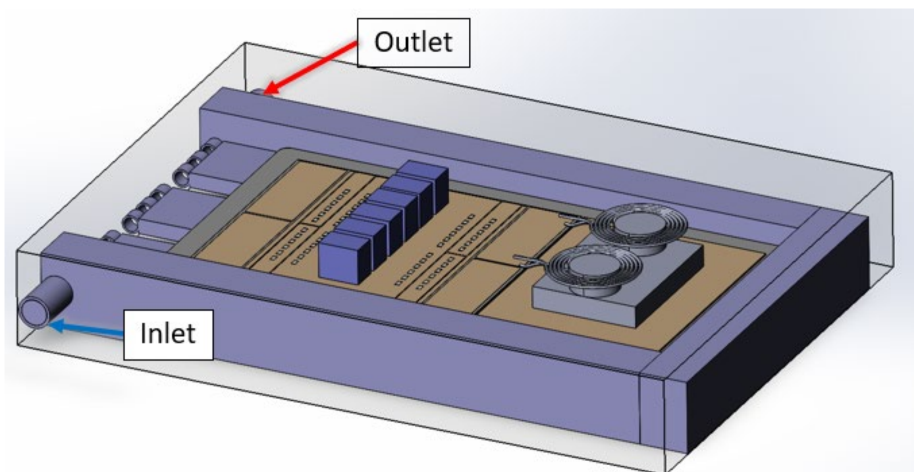

Figure 14: iPEBB thermal model with its computational domain shown. The domain has dimensions of 690mm x 503mm x 101mm and includes all solid components. Note that the inlet and outlet ports are represented by cylindrical caps, onto which the boundary conditions listed are applied.

Solidworks utilizes a volume-based mesh for the subdivision of the domain space. Local areas of high-fidelity mesh were used around the heat generating components of the MOSFETs and transformer core in order to improve the accuracy of results near these critical features.

The conditions for convergence for the solver are the achievement of steady state for the following parameters: inlet surface mass flow rate, outlet surface static pressure, and the temperatures of all solid components.

4. Results and Discussion

Results for the baseline conditions can be seen in Figures 15 and 16. As a reminder, the MOSFETs have a target temperature limit of 150°C, while the transformer core has a target limit of 80°C and acceptable limit of 100°C.

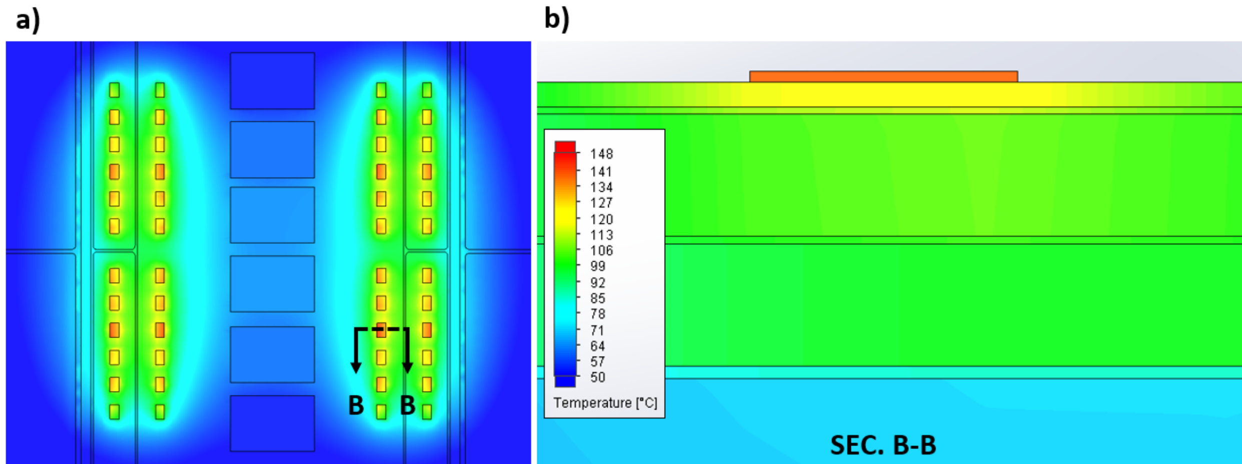

Figure 15: Simulation results for the MOSFETs under the baseline simulation conditions. Shown above are a) top and b) cross-section views of the temperature distribution. The MOSFETs saw a maximum temperature of 148°C. Results for the MOSFETs remain constant when varying the thermal conductivity of ferrite.

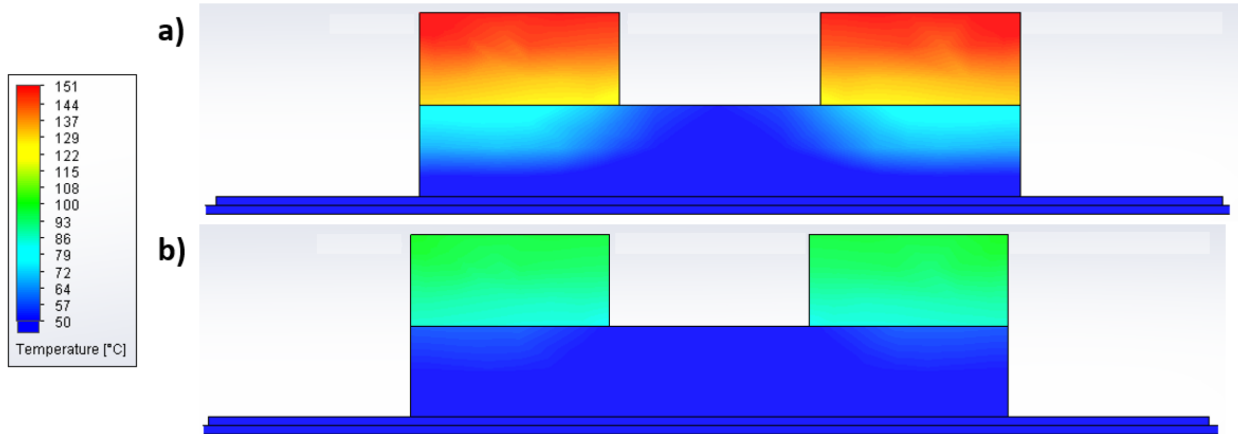

Figure 16: Simulation results for the transformer core under baseline conditions. Cross-section views for when the thermal conductivity of ferrite is set to a) 4 W/m-K and b) 7 W/m-K are both shown. The transformer core saw maximum temperatures of 151°C and 100°C in the two cases respectively. Note the sharp gradient at the line between the cylindrical columns and rectangular base. This is a result of the bodies being modeled as separate volumetric heat sources, with the cylinders having a per-area heat generation rate ~3x higher than the rectangular body.

Following these baseline cases, the simulation was run under three different water inlet temperatures of 15, 25, and 35°C, as well as three application pressures of 5, 10, and 15 psi. Each of these parameters were varied independently, with all other properties and conditions remaining unchanged from the baseline. The forms of the resulting temperature gradients were identical to those of the baseline case; however, the resulting maximum temperatures can be seen in Tables 2 and 3.

Table 2: Simulation Results for Varying Inlet Water Temperatures at 10psi

Inlet Water Temperature [°C]	Max MOSFET Temperature [°C]	Max Transformer Core Temperature [°C]	
		$k_{ferrite} = 4$ W/m-K	$k_{ferrite} = 7$ W/m-K
15	141	143	91
25 (baseline)	148	151	100
35	156	160	109

Table 3: Simulation Results for Varying Application Pressures at 25°C

Application Pressure (psi)	Max MOSFET Temperature [°C]	Max Transformer Core Temperature [°C]	
		$k_{ferrite} = 4$ W/m-K	$k_{ferrite} = 7$ W/m-K
5	155	152	100
10 (baseline)	148	151	100
15	144	151	99

Finally, cases using the baseline conditions were run using the heat pipe configurations described earlier. A third heat pipe setup utilizing both of the outlined concepts simultaneously was also tested. All heat pipe configurations had identical MOSFET results as the baseline case, and therefore temperatures within the transformer core will be focused on. A summary of the heat pipe results can be seen in Table 4. Figures 17, 18, and 19 show a cross-sectional view for each of the heat pipe cases.

Table 4: Simulation Results for Heat Pipe Study at 10psi, 25°C

Configuration	**Max Transformer Core Temperature [°C]**	
	$k_{ferrite}$ **= 4 W/m-K**	$k_{ferrite}$ **= 7 W/m-K**
Baseline, No HPs	151	100
Side HPs	127	86
Imbedded HPs	129	88
4 HPs	118	82

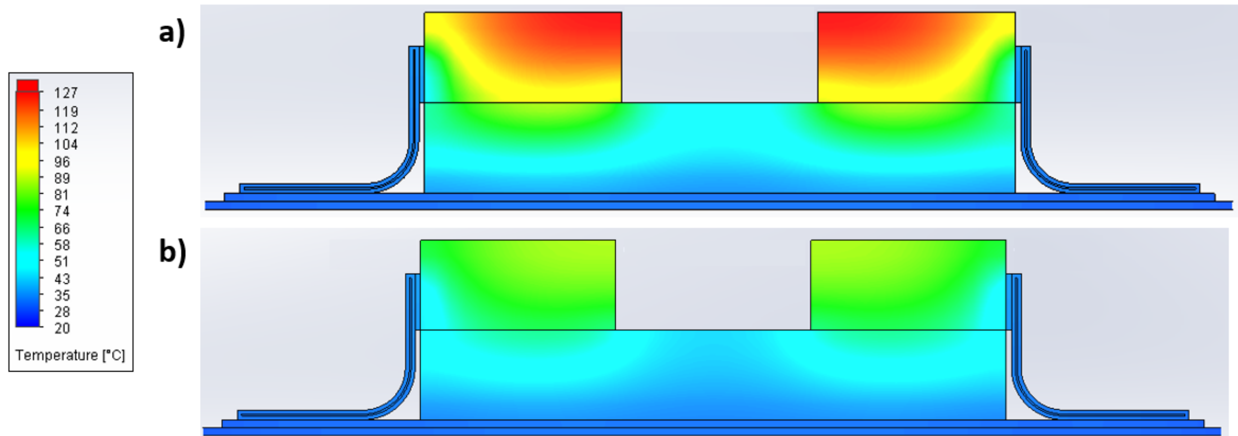

Figure 17: Simulation results for the transformer core with the side heat pipe configuration. Results are shown for both when the thermal conductivity of ferrite is set to a) 4 W/m-K and b) 7 W/m-K. In the $k_{ferrite}$ = 4 W/m-k case, the transformer core reached a maximum temperature of 127°C, 24°C cooler than the baseline. Similarly, the $k_{ferrite}$ = 7 W/m-K scenario saw a 14°C drop in maximum temperature to 86°C.

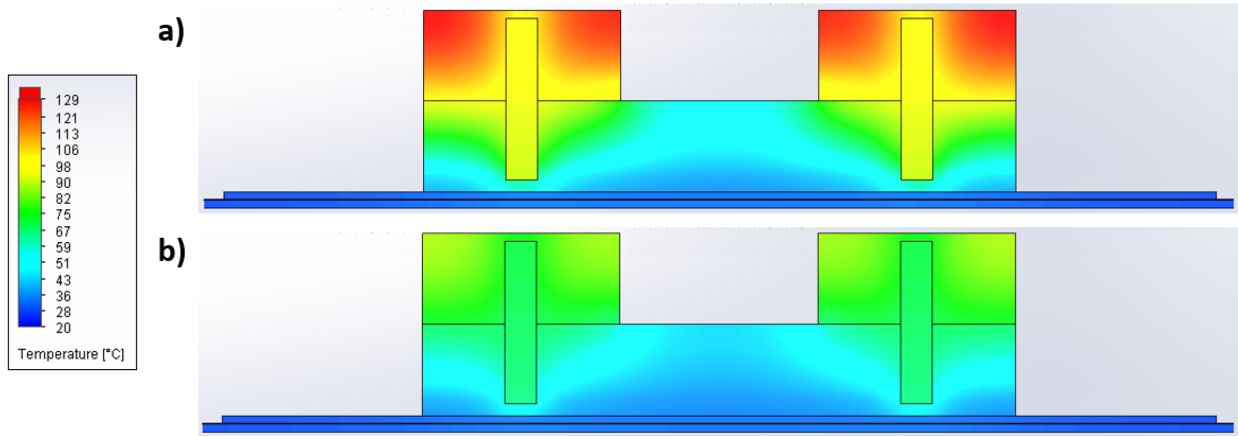

Figure 18: Simulation results for the transformer core with the imbedded heat pipe configuration. Results are shown for both when the thermal conductivity of ferrite is set to a) 4 W/m-K and b) 7 W/m-K. In the $k_{ferrite}$ = 4 W/m-k case, the transformer core reached a maximum temperature of 129°C, a similar trend as in the side heat pipe case with a temperature drop of 22°C from the baseline. Similarly, the $k_{ferrite}$ = 7 W/m-K scenario saw a maximum temperature to 88°C, 12°C below the baseline.

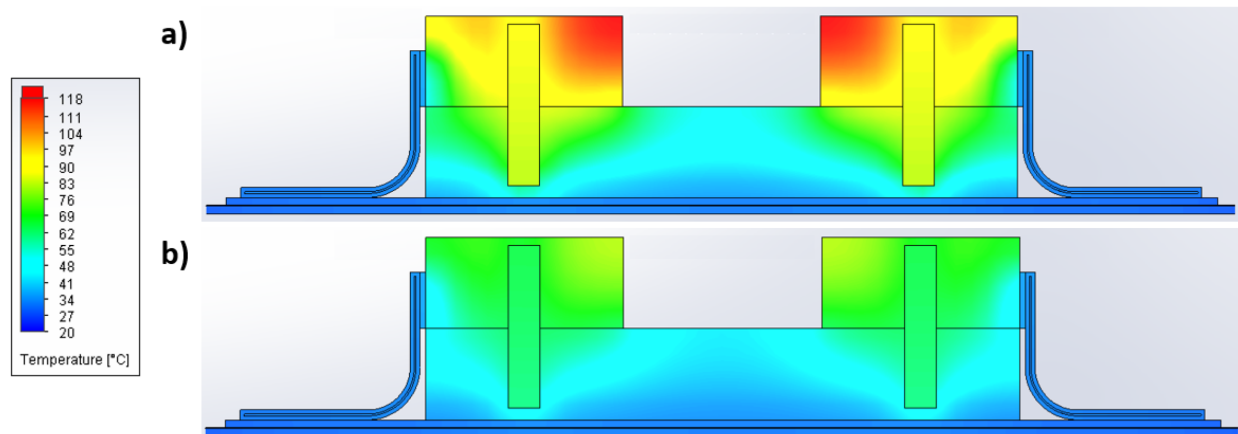

Figure 19: Simulation results for the transformer core with a 4 heat pipe configuration. Results are shown for both when the thermal conductivity of ferrite is set to a) 4 W/m-K and b) 7 W/m-K. This configuration was built from combining the analytical model of the side heat pipes and 1st order model of the imbedded ones. This resulted in maximum core temperatures of 118°C and 82°C in the low and high ferrite thermal conductivity cases respectively.

The baseline results show that the indirect liquid cooling design is capable of maintaining MOSFET temperatures below the target limit of 150°C. Cross-section views show that the common substrate adequately spreads the heat generated from the MOSFET units, overcoming the effects of heat overlap that were an initial area of concern. Stepping into the study of fluid inlet temperature shows that the cold plate as designed, and with a flow rate of 8.4 gpm, is capable of adequately cooling the MOSFETs up to an inlet temperature of 25°C. Varying the application pressure of the PGS thermal interface pad proved to have a large impact on the cooling capability of the fluid flow, with a value of 5 psi resulting in MOSFET temperatures above 155°C. This

sensitivity to the thermal conductivity of the PGS pad shows it presents a bottleneck in the flow of heat from the MOSFETS and to the cold plate.

The baseline cooling configuration, however, fails to maintain areas of the transformer core below 151°C, well above the specification limit of 100°C. The poor heat spreading within the bodies that compose of the core results in high temperatures accumulating towards the regions furthest from the cold plate. While varying inlet water temperatures did affect the cooling performance for the core, indirect liquid cooling remained unable to lower core temperatures to acceptable levels. Varying the application pressure of the PGS pad had little to no effect on core temperatures. It was revealed that the thermal conductivity of the ferrite acts as the dominant source of thermal resistance in the path between the transformer and the cold plate. Testing the ends of the range of thermal conductivity values resulted in a change of 50°C in core temperatures.

Observing the issues with cooling the transformer core inspired the pursuit of the heat pipe concepts, with the goal of supplementing the cooling provided by the cold plate by targeting the warmer, upper areas of the transformer core. The simulations showed that utilizing heat pipes to improve the flow of heat from the warmer regions to the cooled common substrate did succeed in lowering temperatures by over 12°C, however, was unable to cool all areas of the cylindrical bodies for the case of a lower ferrite thermal conductivity ($k_{ferrite}$ = 4 W/m-K).

5. Conclusion and Future Work

The project was conducted with the goal of validating the indirect liquid cooling concept for the thermal management of the Navy iPEBB unit. A computational thermal model was built to mimic the geometry and thermal behavior of an iPEBB half unit, with particular detail given to the 100W per unit heat generating MOSFET switches and 140W generating half-transformer core. Thermal simulations using Solidworks Flow Simulation were used to estimate the temperature distributions under worst-case steady state loading, both under a baseline configuration and with varying inlet water temperatures and mounting application pressures. In addition, three designs using heat pipes were studied as means of assisting with the cooling of the transformer core.

Results showed that the chosen cold plate design with a flow rate of 8.4 gpm, inlet water temperature of 25°C, and unit external application pressure of 10 psi was capable of maintaining MOSFET temperatures to a maximum of 148°C. Reducing inlet water temperature and increasing application pressure on the outer faces of the iPEBB-cold plate system would further increase the positive temperature margin for the switches. The temperature profile of the transformer core was largely dominated by the low thermal conductivity of the ferrite N49 material it is made of, with the bulk geometry contributing to high thermal resistances and concentrations of high temperatures in the cylindrical bodies. Heat pipes were effective at lowering these temperatures, with maximum values between 82°C and 118°C for the 4-heat pipe configuration across the range of thermal conductivities.

The use of heat pipes does result in additional heat losses within the heat pipes, and in the case of the imbedded designs within the transformer core itself; however, these were accounted for within the thermal model using numerical estimates. Overall, heat pipes proved to offer a low-

profile, low-weight method of reducing transformer core temperatures. More work is needed to confirm the implications of such additions on the electrical performance of the iPEBB unit.

The main limitation of the project was the uncertainty surrounding the thermal conductivity of ferrite N49, as the large relative range of likely values resulted in a ~50°C variance in transformer temperatures in cases without heat pipes. Also, the modeling of the heat pipe is considered to be only an approximation of actual performance, however this estimate was made using conservative assumptions. Ultimately the use of conservative assumptions when designing the iPEBB thermal model were taken to offset these concerns. Examples of such decisions include limiting the methods of heat transfer to conduction only through the neglection of convection and radiation, as well as using worst case, steady state heat loads.

Future work for this project would be centered on validating the simulation results through testing of an experimental model. This includes physically verifying the thermal conductivity of the N49 ferrite material. A parallel of this project may include looking into the use of air-cooling within the iPEBB unit for cooling purposes, both independent of and in support of the cold plate design. The results of this paper will serve as a foundation for further modeling work on the iPEBB as well as future analysis of similar applications.

References

[1] Markle, S. P., 2018, "IPES – Harnessing Total Ship Energy & Power." *Sea-Air-Space Exposition, 2018*.

[2] "ESRDC | Electric Ship Research and Development Consortium)" [Online]. Available: https://www.esrdc.com/background/. [Accessed: 22-Apr-2023].

[3] Peterson, L., Schegan, C., Ericsen, T. S., Boroyevich, D., Burgos, R., Hingorani, N. G., Steurer, M., Chalfant, J., Ginn, H., DiMarino, C., Montanari, G. C., Peng, F. Z., Chryssostomidis, C., Cooke, C., and Cvetkovic, I., 2022, *Power Electronics Power Distribution Systems (PEPDS) - Plan.*

[4] Rajagopal, N., 2022, "Navy Integrated Power Electronics Building Block (IPEBB)." *Electric Ship Research and Development Consortium*.

[5] Reyes, I. A., 2022, "Design and Modeling of the Navy Integrated Power and Energy Corridor Cooling System," M.S. thesis, Massachusetts Institute of Technology.

[6] Rajagopal, N., 2021, "Design of 1.7 KV SiC MOSFET Switching Cells for Integrated Power Electronics Building Block (IPEBB)," M.S. thesis, Virginia Polytechnic Institute and State University.

[7] Sharfeldden, S., Raju, R., and DiMarino, C., 2022, "Insulation Design for a Compact, Medium-Voltage Transformer," *2022 IEEE Energy Conversion Congress and Exposition (ECCE),* IEEE, Detroit, MI, USA, pp. 1–6.

[8] 2017, "Ferrites and Accessories - SIFERRIT Material N49." [Online]. Available: https://www.tdk-electronics.tdk.com/download/528856/79b67daa1d54253aa2ae371bb98e9629/pdf-n49.pdf. [Accessed: 15-Mar-2023].

[9] "Basic Properties and Application Examples of PGS Graphite Sheet." [Online]. Available: http://www.mouser.com/pdfdocs/thermalgraphitesheets.pdf. [Accessed: 25-Mar-2023].

[10] Padilla, J., 2023, "Characterizing the Thermal Behavior of Pyrolytic Graphite Sheets (PGS) at Low Interface Pressures," unpublished thesis, Massachusetts Institute of Technology.

[11] Padilla, J., 2023, "PINN Document rev B," unpublished report.

[12] "Heat Pipes for Thermal Management," Advanced Cooling Technologies [Online]. Available: https://www.1-act.com/resources/heat-pipe-resources/faq/. [Accessed: 22-Apr-2023].

[13] Shukla, K. N., 2015, "Heat Pipe for Aerospace Applications—An Overview," JECTC, **05**(01), pp. 1–14.

[14] "EPCOS Data Book 2017 Ferrites and Accessories." [Online]. Available: https://www.mouser.com/datasheet/2/400/ferrites-db-17-pdf-data-1110558.pdf. [Accessed: 10-Apr-2023].

[15] 2022, "'GraphiteTIM (Compressible Type)' PGS with Low Thermal Resistance EYGS, EYGR Type."

[16] "IGBT Cold Plates - High Performance." [Online]. Available: https://www.qats.com/Products/Liquid-Cooling/Cold-Plates. [Accessed: 09-Apr-2023].

[17] Ordonez-Miranda, J., Hermens, M., Nikitin, I., Kouznetsova, V. G., van der Sluis, O., Ras, M. A., Reparaz, J. S., Wagner, M. R., Sledzinska, M., Gomis-Bresco, J., Sotomayor Torres, C. M., Wunderle, B., and Volz, S., 2016, "Measurement and Modeling of the Effective Thermal Conductivity of Sintered Silver Pastes," *International Journal of Thermal Sciences*, 108, pp. 185–194.

[18] "Heat Pipe Calculator | Copper Water Heat Pipes," Advanced Cooling Technologies Inc. [Online]. Available: https://www.1-act.com/resources/heat-pipe-calculator/. [Accessed: 22-Apr-2023].

[19] Advanced Cooling Technologies Inc, "Heat Pipe Design and Modeling Techniques", *YouTube*, 25-June-2021. Available: https://www.youtube.com/watch?v=Shisfff7ulM [Accessed: 15-Mar-2023]

[20] Hein, H., Yue, S., and Li, Y., 2019, "Comparative Core Loss Calculation Methods for Magnetic Materials under Harmonics Effect," IOP Conf. Ser.: Mater. Sci. Eng., **486**(1), p. 012019.

[21] "Thermally Conductive Epoxy Adhesives," MasterBond [Online]. Available: https://www.masterbond.com/properties/thermally-conductive-epoxy-adhesives. [Accessed: 22-Apr-2023].

Appendix

Temperature-dependent Thermal Conductivity Tables for Selected Materials:
(All sourced from Solidworks Engineering Database Library)

Silicon Carbide (SiC):

Temperature	Thermal conductivity
293 K	150 W/(m*K)
473 K	126.6 W/(m*K)
673 K	77.5 W/(m*K)

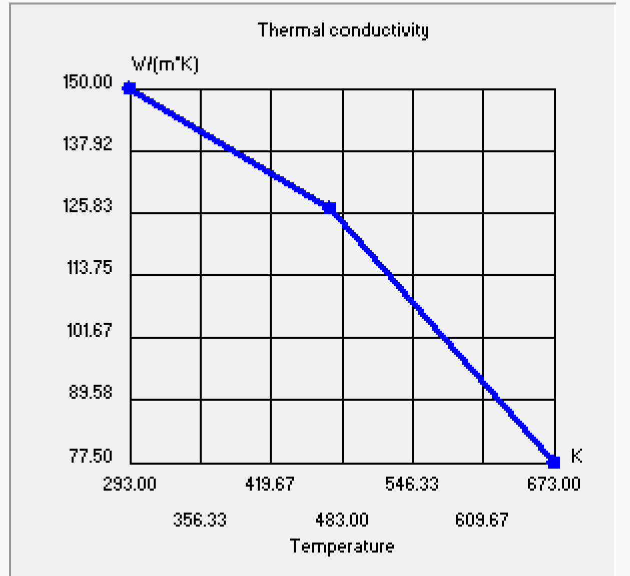

Copper:

Temperature	Thermal conductivity
4 K	16200 W/(m*K)
10 K	24000 W/(m*K)
20 K	10800 W/(m*K)
40 K	2170 W/(m*K)
80 K	560 W/(m*K)
150 K	429 W/(m*K)
200 K	413 W/(m*K)
300 K	401 W/(m*K)
400 K	393 W/(m*K)
600 K	379 W/(m*K)
800 K	366 W/(m*K)
1000 K	352 W/(m*K)
1356.2 K	327 W/(m*K)

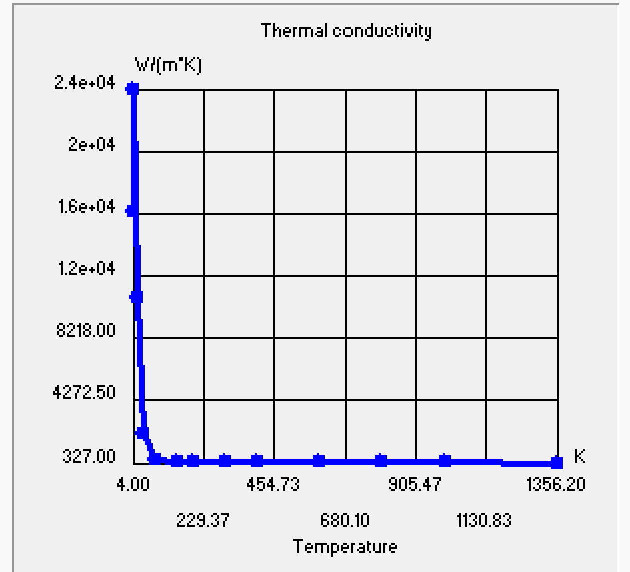

Aluminum (unfinished):

Temperature	Thermal conductivity
4 K	15700 W/(m*K)
10 K	23500 W/(m*K)
20 K	11700 W/(m*K)
40 K	2400 W/(m*K)
80 K	430 W/(m*K)
150 K	248 W/(m*K)
200 K	237 W/(m*K)
300 K	237 W/(m*K)
400 K	240 W/(m*K)
600 K	230 W/(m*K)
800 K	220 W/(m*K)
933.4 K	225 W/(m*K)

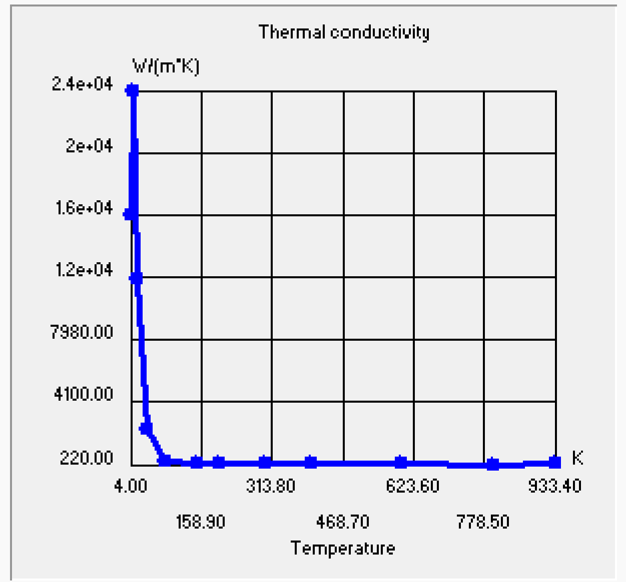

Resistor Network for Transformer Cylinder Core (with Side Heat Pipes):

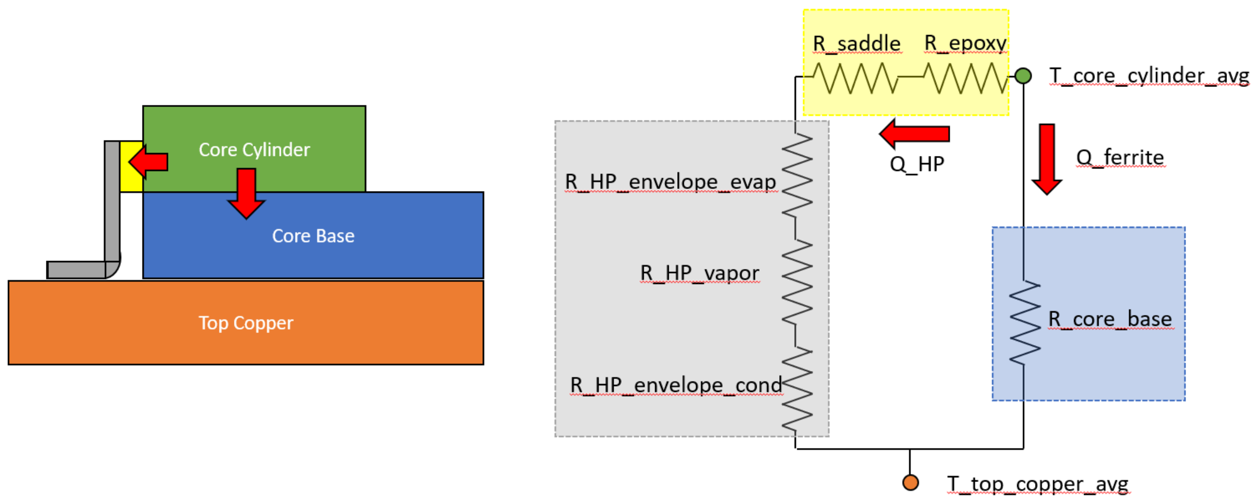

Saddle Resistance:

$$R_{epoxy} = \frac{L}{k_{epoxy}A} = \frac{15 \times 10^{-6}m}{(2.1\frac{W}{mK})(1.64 \times 10^{-4}m^2)} = 0.0435\ K/W$$

$$R_{saddle} = \frac{L}{k_{copper}A} = \frac{0.002m}{(380\frac{W}{mK})(1.63 \times 10^{-4}m^2)} = 0.0324\ K/W$$

Heat Pipe Resistance:

$$R_{HP,envelope,evap} = \frac{L}{k_{env}A} = \frac{0.001m}{(26.67\frac{W}{mK})(1.63 \times 10^{-4}m^2)} = 0.234\ K/W$$

$$R_{HP,vapor} = \frac{L}{k_{vap,4}A} = \frac{0.0518m}{(80309\frac{W}{mK})(3.04 \times 10^{-6}m^2)} = 0.212\ K/W$$ (for $k_{ferrite}$ = 4 W/m-K)

$$R_{HP,vapor} = \frac{L}{k_{vap,7}A} = \frac{0.0518m}{(67844\frac{W}{mK})(3.04 \times 10^{-6}m^2)} = 0.251\ K/W$$ (for $k_{ferrite}$ = 7 W/m-K)

$$R_{HP,envelope,cond} = \frac{L}{k_{env}A} = \frac{0.001m}{(26.67\frac{W}{mK})(3.67 \times 10^{-4}m^2)} = 0.104\ K/W$$

Ferrite Resistance:

$$R_{ferrite} = \frac{L}{k_{f4}A} = \frac{0.023m}{(4\frac{W}{mK})(0.0025m^2)} = 2.30\ K/W$$ (for $k_{ferrite}$ = 4 W/m-K)

$$R_{ferrite} = \frac{L}{k_{f7}A} = \frac{0.023m}{(7\frac{W}{mK})(0.0025m^2)} = 1.31\ K/W$$ (for $k_{ferrite}$ = 7 W/m-K)

Finding Heat Flow (for $k_{ferrite}$ = 4 W/m-K):

$$R_{HP} = 0.63\ K/W$$

$$R_{core} = 2.30\ K/W$$

$$Q_{HP} = Q_{total}\frac{R_{core}}{R_{core} + R_{HP}} = 23.6W$$

$$Q_{core} = Q_{total} - Q_{HP} = 6.4W$$

Finding Heat Flow (for $k_{ferrite}$ = 7 W/m-K):

$$R_{HP} = 0.67\ K/W$$

$$R_{core} = 1.31\ K/W$$

$$Q_{HP} = Q_{total}\frac{R_{core}}{R_{core} + R_{HP}} = 19.9W$$

$$Q_{core} = Q_{total} - Q_{HP} = 10.1W$$

Temperature-dependent Properties for Deionized Water:
(sourced from Solidworks Engineering Database Library)